

Ultralow Dissipation Nanomechanical Devices from Monocrystalline Silicon Carbide

Leo Sementilli,^{1,*} Daniil M. Lukin,^{2,*} Hope Lee,² Erick Romero,¹ Jelena Vučković,^{2,†} and Warwick P. Bowen^{1,3}

¹*The Australian Research Council Centre of Excellence for Engineered Quantum Systems, School of Mathematics and Physics, University of Queensland, St. Lucia, Queensland 4072, Australia*

²*E. L. Ginzton Laboratory, Stanford University, Stanford, California 94305, USA*

³*The Australian Research Council Centre of Excellence in Quantum Biotechnology, School of Mathematics and Physics, University of Queensland, St. Lucia, Queensland 4072, Australia*

Due to their low mass and long coherence times, nanomechanical resonators have many applications, from biomolecule mass sensing to hybrid quantum interfaces. In many instances the performance is limited by internal material damping. Crystalline materials promise lower material dissipation, however due to fabrication challenges, amorphous materials are more commonly utilized. Crystalline silicon carbide (SiC) is particularly appealing due to its exquisite mechanical, electrical and optical properties, but to-date exhibits higher nanomechanical dissipation than both amorphous and other crystalline materials. To address this, we fabricate nanomechanical resonators thinned from bulk monocrystalline 4H-SiC. Characterization of multiple resonators of different sizes and thicknesses, allows us to discern the surface and volumetric contributions to dissipation. We measure mechanical dissipation rates as low as 2.7 mHz, more than an order-of-magnitude lower than any previous crystalline SiC resonator, yielding quality factors as high as 20 million at room temperature. We also quantify the nonlinear dissipation of SiC nanomechanical resonators for the first time, finding that it is lower than other materials. This promises higher sensitivity in applications such as mass sensing. By achieving exceptionally low dissipation in SiC resonators, our work provides a path towards improved performance in sensing and other applications.

I. INTRODUCTION

Nanomechanical resonators play a significant role in modern day technologies and fundamental scientific research. They are applied as nanoscale sensing probes in biological environments [1, 2], radio and microwave frequency timing and filtering elements in MEMS [3, 4], as well as on-chip navigation and position awareness devices [5, 6]. In many cases the mechanical dissipation rate is a key figure of merit. The mechanical dissipation rate directly determines the thermomechanical noise of an oscillator and the minimum resolvable oscillator displacement above this noise floor [7]. In nanomechanical resonators it is commonly set by friction effects in the material from which the resonator is fabricated. This material dependent damping is quantified using the intrinsic quality factor, Q_{int} , of the resonator [8].

Compared to amorphous counterparts, pure crystalline materials have a higher intrinsic quality factor (less material dissipation) because of their defect-free and structured atomic lattice. However, fabricating resonant devices from them is challenging. For nanoscale resonators, these challenges involve the material growth and processing of samples, as well as nanofabrication processes undertaken to produce devices and thin films defect-free. Further, nanomechanical resonators possess additional mechanical loss mechanisms, such as surface loss, which are less relevant in larger scale resonators.

These challenges have been addressed in crystalline nanomechanical resonators based on diamond and sili-

con thin films, shown to exhibit intrinsic damping drastically lower than defect-rich crystalline and amorphous materials [9, 10]. Another attractive crystalline material platform is silicon carbide (SiC). Silicon carbide is similar to diamond in that it has high material yield strength [11, 12], and hosts color centers used for quantum photonics [13, 14]. Also much like silicon, SiC has high quality photonic properties [15–17], and is mass manufactured in industrial settings, and sold as an affordable semiconductor. Further, silicon carbide has a high thermal conductivity and wide electronic bandgap [18], making it an ideal material for electrical and MEMS devices. Despite these attractive properties, nanomechanical resonators based on crystalline thin film silicon carbide have been found to have intrinsic quality factors orders-of-magnitude lower than the predicted volumetric limit [19–22].

Previous approaches use silicon carbide thin films grown directly on silicon substrates, which possess different crystalline structure and therefore lattice spacing [19, 20]. It is well known that this process introduces an interfacial defect layer [23, 24]. Indeed, this is necessary for the crystal growth process. In 3C-SiC nanomechanical resonators, the defect layer has been found to introduce additional dissipation [20]. Even with its removal, the dissipation of nanomechanical resonators fabricated from 3C-SiC is still more than an order-of-magnitude away from the currently known volumetric damping limit of silicon carbide [20]. To address this, we explore nanomechanical resonators fabricated from 4H-monocrystalline SiC. We utilize bulk sublimation grown silicon carbide crystals, and a grind-and-polish technique to achieve defect-free thin films. By characterizing various cantilever and string resonators of different sizes

* These authors contributed equally to this work.

† jela@stanford.edu

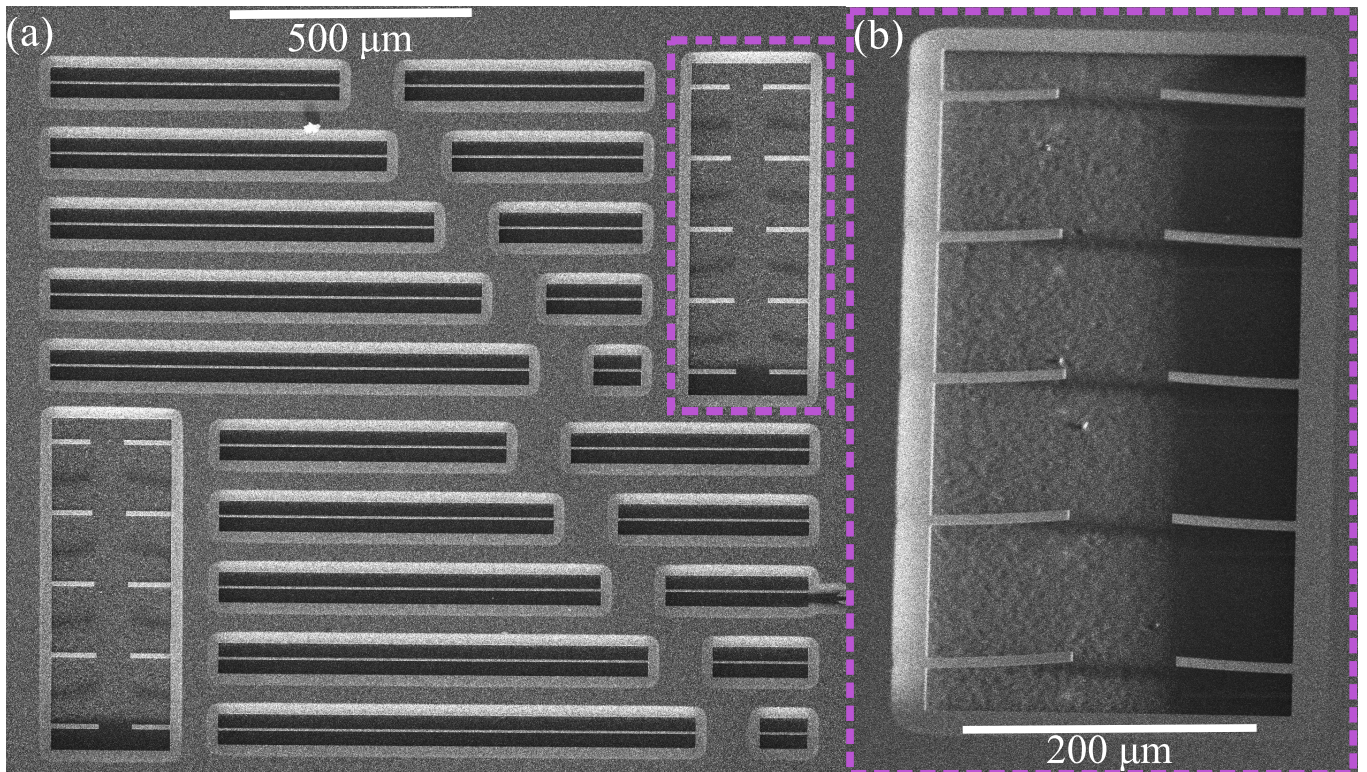


Figure 1. (a) SEM image of arrays of uniform nanomechanical string and cantilevers used for material characterization. Width of devices is kept constant to $5\mu\text{m}$, whereas the lengths of both cantilevers and strings are varied. The purple dashed box encompasses the array of cantilevers highlighted in (b). (b) Higher magnification SEM image of nanomechanical cantilevers with different lengths.

and thicknesses, we find that this fabrication approach greatly reduces the intrinsic damping of crystalline silicon carbide nanomechanical resonators. We achieve dissipation rates as low as 2.7 mHz, and quality factors as high as 20 million at room temperature with devices possessing only a few hundred megapascals of tensile stress. The total material intrinsic damping that we achieve is an order-of-magnitude lower than silicon carbide nanomechanical resonators fabricated from heteroepitaxially grown crystals [20], and nearly two orders-of-magnitude lower than bulk crystalline silicon carbide resonators [25]. We find that the volumetric dissipation reaches the reported material limit [8, 26], and is the dominant dissipation mechanism for thick resonators. Finally, the low linear dissipation of our devices allows us to observe and quantify nonlinear dissipation in crystalline silicon carbide nanomechanical resonators for the first time. We find that the nonlinear dissipation is lower than other materials such as amorphous silicon nitride. This is important for applications where nonlinear effects constrain performance, such as mass sensing [27, 28], and nanomechanical computing [29, 30]. We anticipate the ultralow dissipation mechanical properties of crystalline silicon carbide that we observe will promote the materials use in a range of future technologies.

II. DEVICE FABRICATION

Crystalline silicon carbide can exist in hundreds of polytypes, forming different crystal structures. The most commonly manufactured and studied are cubic (3C) and hexagonal (4H, 6H) crystalline configurations [31]. As the most technologically mature and available polytype, 4H has been used for spin qubit systems [32], integrated photonics [16, 17], bulk acoustic wave resonators [25], and micro-electromechanical devices [33]. However, 4H-SiC has largely been unexplored as a material platform for nanomechanical resonators, with most work to date being conducted on the polycrystalline 3C polytype [19–21]. Previous research has been focused on the 3C polytype because of the availability of commercial heteroepitaxially grown high deposition stress wafers ($> 1\text{GPa}$) on silicon substrates [19, 20]. Specifically, the belief was held that high tensile stress would lead to high quality factors through dissipation dilution techniques in a similar way to silicon nitride on silicon wafers [34, 35]. Nonetheless, the lattice mismatch between 3C-SiC and the silicon substrate which enables high tensile stress, imposed a crucial trade-off in material quality, increasing the density of crystalline defects, resulting in low intrinsic quality factors [20, 21]. Unlike 3C, the 4H polytype is not grown on a different material substrate, and is in-

stead grown using silicon carbide crystals as a seed layer. The result of this growth process is a single pure crystalline material, which is then bonded to a substrate for processing. This offers an advantage over the 3C polytype as there is no interfacial defect layer from the film growth process. Further, the 4H polytype is monocrystalline, meaning the crystal lattice possesses less grain boundaries and stacking faults compared to polycrystalline 3C. Both of these factors could be expected to reduce mechanical dissipation within the material itself as the crystal lattice vibrates. Here, we investigate this by fabricating and studying nanomechanical resonators using the 4H-SiC polytype.

The devices studied here are fabricated using a process consisting of thin film preparation, metal deposition, electron beam patterning, reactive ion etching, and dry selective release. The samples are first derived from bulk crystalline 4H-SiC wafers, which are then thermally bonded onto silicon carrier wafers via a thin (160 nm) bonding silicon oxide layer. The bonded SiC film is then thinned to sub-micron thickness using the grind and polish technique [16]. This technique, developed in recent years, has enhanced crystalline thin film quality, enabling low-loss integrated photonics in 4H-SiC and diamond [16, 36], as well as, most recently, on-chip titanium-sapphire lasers [37]. Despite the better film quality, thickness uniformity across wafer scales remains an outstanding challenge. In this study, the thinning process results in thickness nonuniformity of approximately 10-20 nm per millimeter of resonator length across our sample which is determined using optical thin film profiling techniques. To account for this, mechanical resonators are selectively patterned within regions of largest mapped uniformity. The mean device thickness is then found across each resonators thickness profile and used for analysis purposes.

After the preparation of the crystalline thin film, aluminium is evaporated on the silicon carbide layer to act as a hard mask for etching. Following this, device geometries are initially realized using electron beam lithography, then formed using reactive ion etching of the aluminium, silicon carbide, and silica layers. The aluminium is then stripped chemically, and the devices are undercut using XeF₂ dry etching. This leaves 4H-SiC structures suspended with thermal silica still adhered to the bottom interface of the devices. The remaining thermal silica is then removed using vapor HF, resulting in freestanding structures that are purely 4H-SiC. SEM images of near complete devices are presented in Figures 1(a-b), needing only the last vapor HF step.

III. RESULTS

To thoroughly characterize the nanomechanical dissipation of the 4H-SiC material, we use uniform width cantilever and string structures, whose simple geometries make analytic calculations of resonant frequencies

and dissipation dilution factors possible [7, 38]. Furthermore, we conduct this analysis over a wide range of device thicknesses, allowing us to form an intrinsic quality factor (Q_{int}) model comprised of volume (Q_{vol}) and thickness (h) dependent surface (Q_{surf}) loss component as described by [20, 39]

$$Q_{\text{int}}(h) = (Q_{\text{vol}}^{-1} + (Q_{\text{surf}} \cdot h)^{-1})^{-1}. \quad (1)$$

We characterize the dissipation of the resonators using ringdown measurements in an optical heterodyne detection setup at infrared wavelengths (780 nm) under high vacuum ($\approx 10^{-6}$ mbar) [19, 20]. Using this scheme we first measure thermal motion spectra, then employ external piezo driving at the mechanical resonance frequencies to excite the resonators to higher oscillation amplitudes. The external drive piezos are then turned off and the decay of resonator's oscillation amplitude is subsequently monitored with the interferometric detection. An experimental trace of a ringdown measurement is shown in Figure 2(a). This ringdown allows us to determine the quality factor of the mechanical mode, and extract the mechanical dissipation rate. We repeat this process to extract multiple ringdown traces (between 2-5) for each device.

A. Cantilevers

Uniform cantilever structures are among the simplest mechanical resonators to study because of the lack of tensile stress. This implies that there will be no dissipation dilution and therefore the resonators are subject to only intrinsic and radiation loss (assuming no gas damping). The acoustic radiation loss of a cantilever can be determined using an analytical approximation [8], from which we estimate our cantilevers with the most significant radiation loss to have a radiative quality factor limit of roughly 10^{10} . As the measured quality factors are several orders-of-magnitude removed from this limit we neglect this contribution in our analysis. Under this assumption, the measured quality factor of the cantilevers are in fact the intrinsic quality factor.

Measurements are conducted on 18 different cantilever resonators of constant width (5 μm), device lengths between 80–100 μm , and device thicknesses over a range of 180–500 nm. We plot the average intrinsic quality factor measurements as a function of device length and thickness in Figure 2(b-c). Each data point here represents an individual device, with error bounds composed of the standard deviation of measured quality factors for the fundamental mode among multiple traces. We measure a maximum intrinsic quality factor greater than $2 \cdot 10^4$, with the quality factor of many devices exceeding 10^4 .

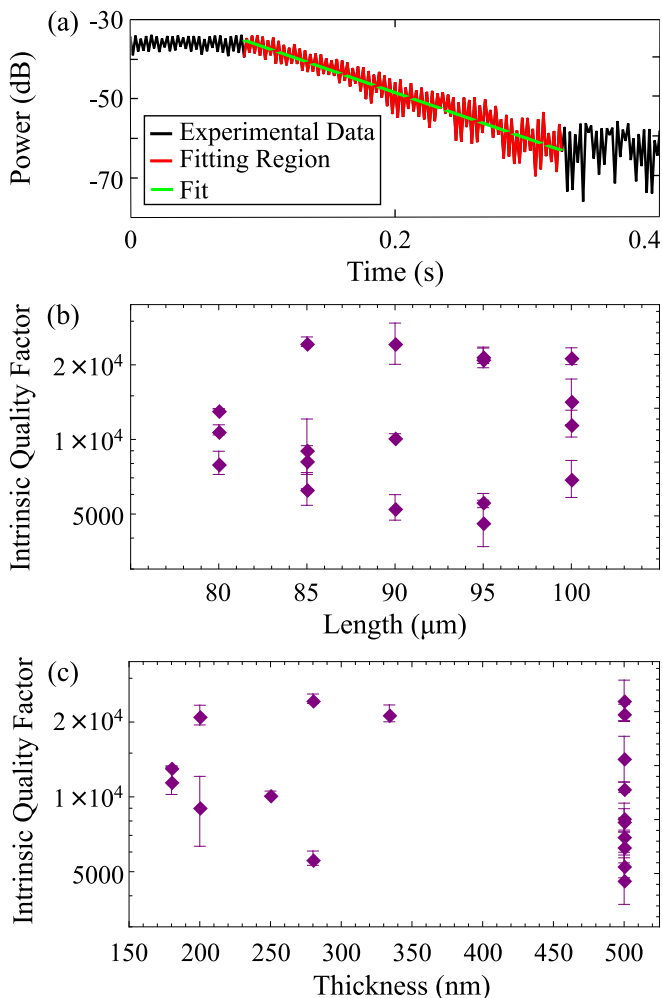


Figure 2. (a) Ringdown measurement of one cantilever device. The red fitting region represents free decay of the oscillator, specifically when there is no external drive. In this experimental trace, we fit a quality factor of $2 \cdot 10^4$ for a fundamental mode at 41.5 kHz. (b) Intrinsic quality factor versus length of cantilever nanomechanical resonators. (c) Intrinsic quality factor versus thickness of cantilever nanomechanical resonators. Each point represents an individual device with error bounded by the standard deviation of many ringdown measurements.

B. Nanostrings

We next characterize two sets of uniform-width string resonators. In total we characterize 50 of them across two separately prepared samples, with a variety of device thicknesses, lengths, widths and tensile stresses. The geometrical sizes of the devices are controlled via device design and fabrication, while the tensile stress is the result of different manifested stresses originating in the thin film preparation between different sample chips.

The first set of uniform strings is fabricated on the same sample as the cantilever devices, as shown in Figure 1(a). In this device set, the lengths and thicknesses of the string resonators vary, and the device widths are

constant. The second sample set of uniform strings consists of larger aspect ratio devices, all of the same length and width, with a smaller thickness range among the device set (100 – 135nm). As a result of the very different device parameter sweeps and intrinsic stress values, we first analyze the sample sets separately, then ultimately combine the data in Section III C. From here, we distinguish the samples by referring to them as “characterization strings” and “high aspect ratio strings”, respectively.

1. Characterization Strings

Within the first uniform string sample set we measure 30 string resonators of consistent 5 μm width, whose lengths vary between 100 μm and 1000 μm, and thicknesses span between 400 nm and 815 nm. We plot the average and standard deviation of the quality factor of the fundamental transversal mode of each device as a function of length in Figure 3(a). The measured quality factors, as high as $Q = 8.0 \cdot 10^5$, exceed those found in cantilever resonators due to the presence of tensile stress and therefore dissipation dilution. The resonance frequency of a string resonator of length and material density, L and ρ , is related to the tensile stress, σ by [8]

$$f = \frac{n}{2L} \sqrt{\frac{\sigma}{\rho}}. \quad (2)$$

Thus, the intrinsic tensile stress of each device can be determined by its resonance frequency. To determine the mean intrinsic tensile stress of the entire data set, we plot the inverse of the resonance frequency against length in Figure 3(b). As expected from Equation 2, the data lies on a line. A fit then provides the mean stress of roughly $\sigma = 172$ MPa after release.

In contrast to the cantilever resonators, we find that the string resonators exhibit non-negligible radiation loss. The radiation loss of the fundamental mode of a string resonator follows [20]

$$Q_{\text{rad}} = \alpha \frac{3\rho_s}{2\rho} \sqrt{\frac{E_s \rho}{2\sigma \rho_s}} \frac{L}{h}. \quad (3)$$

In this model, ρ_s and E_s represent the density (2650 kg/m³) and Young’s Modulus (170 GPa) of the silicon substrate. We determine the fitting parameter $\alpha = 317$ based on a least-square fits of the intrinsic quality factor as a function of alpha ($Q_{\text{int}}(h, \alpha)$), conducted and discussed further in Section III C. The green curve in Figure 3(a) shows the radiation loss quality factor limit for the thickest devices. This represents the highest radiation loss among the “characterization strings” data set, and the shaded region beyond this curve encompasses the radiation loss expected for thinner devices. It is apparent from Figure 3(a) that the devices are not at the radiation loss limit but the radiation loss is non-negligible.

For example, for the 400 μm long string with the highest quality factor ($Q = 6.5 \cdot 10^5$), radiation loss accounts for approximately 8.5% of the total loss. As such, radiation loss will be included in the intrinsic damping model of 4H-SiC discussed in Section III C.

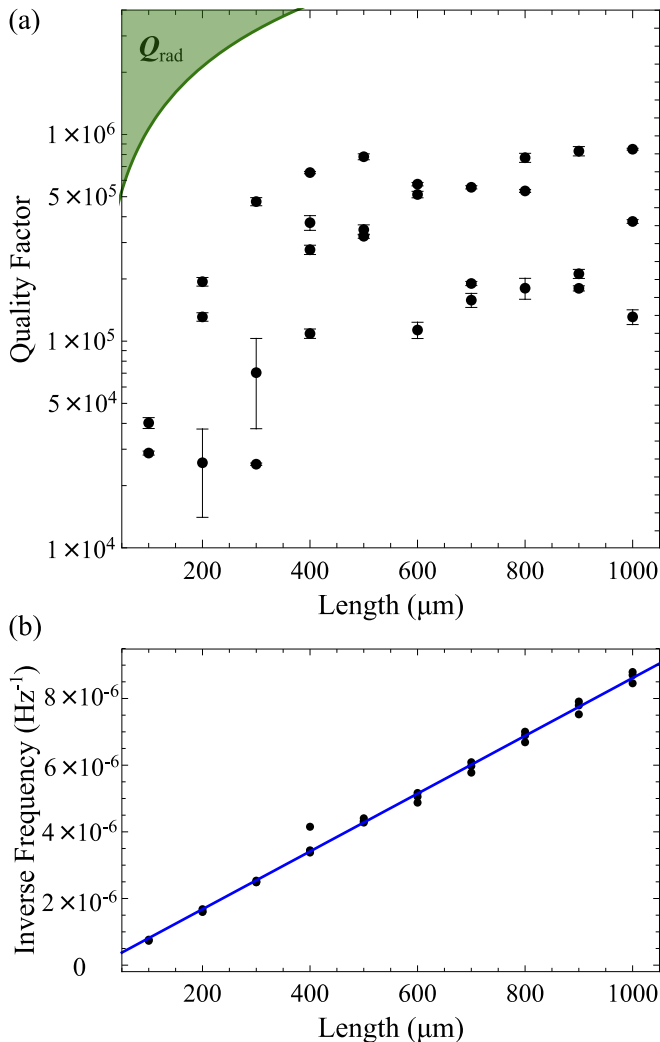


Figure 3. (a) Quality factor versus length of uniform string nanomechanical resonators. Here each point represents an individual device with error bounded by the standard deviation of many ringdown measurements. The green curve represents the quality factor limit associated with radiation loss (Q_{rad}) for devices with largest damping due to this loss (thickest). (b) Inverse resonance frequency as a function of string resonator length, where each point represents an individual device's fundamental transversal resonance frequency and the blue line represents the expected resonance frequency using the analytical model in Equation 2, and extracted mean stress of the devices (172 MPa).

2. High Aspect Ratio Strings

To achieve the largest possible quality factor in simple resonator geometries, uniform string resonators with larger aspect ratios are prepared on a separate sample to the cantilevers and characterization strings presented earlier. These devices all possess a constant uniform width (800 nm), with a fixed length of 3.1 millimeters and thicknesses between 110-135 nm. We perform ringdown measurements for the first three transversal modes of 20 uniform string devices ($n = 1, 2, 3$ in Equation 2). An example ringdown measurement is shown in Figure 4(a) (for the red colored point in (b)), for a 53 kHz fundamental transversal mode with $Q = 1.5 \cdot 10^7$. The quality factor for each mode of the device set is plotted in Figure 4(b) as a function of resonance frequency. The gray shaded regions represent the expected eigenfrequency range deduced from the thickness span of the device set, and inferred minimal and maximal stress based on the fundamental transversal resonance frequency (290 MPa - 335 MPa). It is evident that the measured eigenfrequencies are consistent with predictions across multiple modes over all 20 devices. Quality factors exceeding 10^7 are measured in the first three transversal modes among a few different string resonators. These quality factor are nearly an order of magnitude larger than other crystalline SiC string and trampoline nanomechanical resonators in the literature [20, 21, 40]. The mechanical dissipation rate ($\Gamma/2\pi$, $f/Q = 3.5$ mHz) of this trace is also a factor of 27 times better than the best reported in 3C-SiC strings [19]. When exploring the nonlinear dissipation of this device in Section V, we measure a mode with an even higher quality factor of $2 \cdot 10^7$, and lower dissipation rate of 2.7 mHz. This ringdown yields a $Q \cdot f$ product of $1 \cdot 10^{12}$. Even though the device is under a factor of 5 times less stress, this exceeds the highest reported $Q \cdot f$ product in high stress crystalline 3C-SiC nanostrings [19].

C. Intrinsic Linear Dissipation Model

Using the measurements compiled from our three sample sets we are able to form an intrinsic dissipation model. While intrinsic quality factors can be directly inferred from the cantilever devices, string resonators possess dissipation dilution which enhances quality factors above the material damping limits [19, 20, 41]. As a result, to accurately determine the material damping we fit a dissipation dilution factor for each string resonator based on its own determined intrinsic stress and device dimensions (as well as undercut, the effect of which was determined using finite element modeling - see Supplemental). The dissipation dilution factor for each device is determined using the analytical solution [8, 42]

$$D \approx \left[\frac{(n\pi)^2 E}{12 \sigma} \left(\frac{h}{L} \right)^2 + \frac{1}{\sqrt{3}} \sqrt{\frac{E}{\sigma}} \left(\frac{h}{L} \right) \right]^{-1}, \quad (4)$$

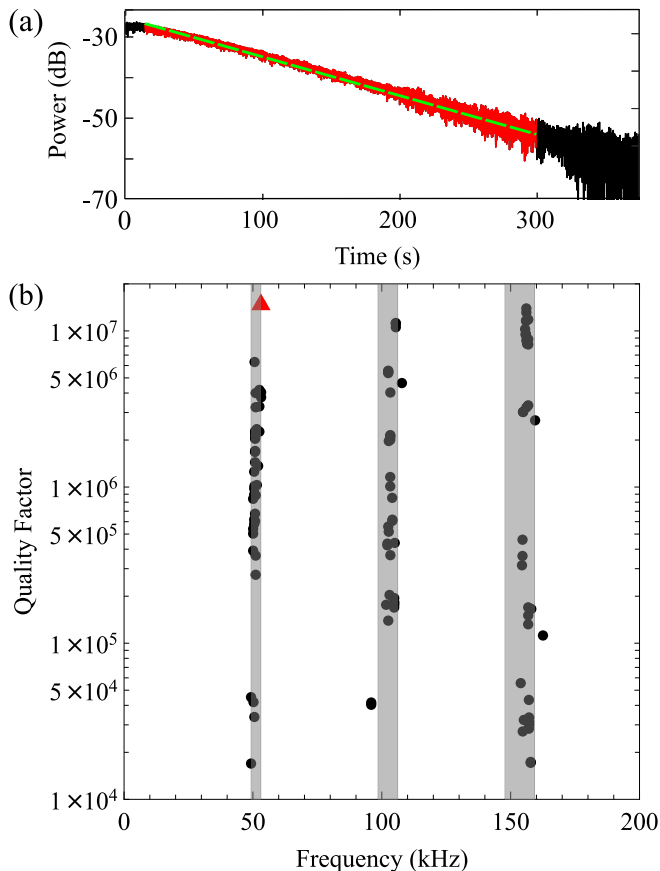


Figure 4. (a) Ringdown measurement of a device with a quality factor exceeding 10^7 at 53 kHz. (b) $Q \cdot f$ map for the first three transversal modes of 20 high aspect-ratio nanomechanical strings. The shaded gray regions represent the expected frequency range based on device dimensions and tensile stress. The red colored point represents the measurement shown in (a).

which applies to a uniform string nanomechanical resonator under tensile stress. Using Equation 4, and the relationship between intrinsic quality factors and dissipation diluted quality factors ($Q_D = Q_{\text{int}} \times D$), we extract an intrinsic quality factor for string resonators of

$$Q_{\text{int}} = (D \times (Q_D^{-1} - Q_{\text{rad}}^{-1}))^{-1}, \quad (5)$$

where Q_{rad} is the radiation loss limited quality factor introduced in Equation 3. We include this loss mechanism for all strings in both data sets, using each device dimension and intrinsic stress inferred from the fundamental transversal eigenfrequency. We then plot the extracted string resonator intrinsic quality factors alongside our cantilever quality factors from Figure 2(b), in Figure 5. In this figure string resonators are represented with circular points, while the cantilevers are differentiated with diamond points. More than 20 devices have intrinsic quality factors above 10^4 , including at least one device from each of the three sample sets. The maximum intrinsic quality factor from the data is $4.2 \cdot 10^4$ in

a 500 nm thick string resonator. Additionally, we see no significant differences in intrinsic quality factors between cantilever and string geometries. This is expected as intrinsic quality factors are only dependent on a resonator's surface-to-volume ratio and not dependent on resonator type [8]. Further, this indicates that our dissipation dilution and radiation loss model of string resonators are appropriate for the devices being studied here. We do observe an increase in intrinsic quality factor with an increase in device thickness, meaning surface losses become less important as the surface area to volume ratio of the devices decreases. This trend is expected as it has been commonly observed in silicon nitride [39], and is well understood from other nanomechanical studies [20, 43, 44].

To determine the upper limit of the intrinsic quality factor, a least-square fit is performed among the five red data points with black boundaries in Figure 5. We choose these five points because they represent the highest measured intrinsic quality factors at different device thicknesses. They therefore provide information about the highest intrinsic quality factors achieved for the 4H-SiC nanomechanical resonators in this study. Among these points is at least one device from each of the three device sets studied here (cantilevers, characterization strings, high aspect ratio strings). We consider both intrinsic volume and surface dissipation in our fit, as well as dissipation from radiation loss, following the process from Reference [20]. This allows us to quantify each dissipation mechanism, and identify their contribution to the overall intrinsic quality factor. The least-square fit uses the standard nanomechanical volume and surface dissipation model introduced in Equation 1, with an additional fitting parameter α , from Equation 3, which accounts for radiation loss of string resonators. This fit yields $Q_{\text{vol}} = 1.5 \cdot 10^5$, $Q_{\text{surf}} = 11.5 \cdot 10^{10} \text{ m}^{-1} \cdot h$, and $\alpha = 317$, which is plotted as a red dashed line in Figure 5. This suggests that surface loss becomes the dominating intrinsic loss mechanism at roughly 1300 nm thickness. The highest observed volumetric quality factor of our resonators is consistent with the theoretical material limit ($1 \cdot 10^5$) based on the material loss tangent of silicon carbide [8, 26]. Other resonators within our study do not reach this limit, potentially due to local crystalline imperfections in the thin films used, or contamination during the fabrication process. The difference between predicted and measured volumetric quality factors is difficult to explain but may be due to small thin film thickness variation across our devices.

IV. COMPARISON WITH STATE-OF-THE-ART

The intrinsic quality factors of nanomechanical resonators varies orders-of-magnitude between different material types and film quality [8, 9, 20]. The use of cryogenics and device surface treatments have been shown to enhance intrinsic quality factors [9, 10, 46]. Since we make use of neither technique in this work, the comparisons

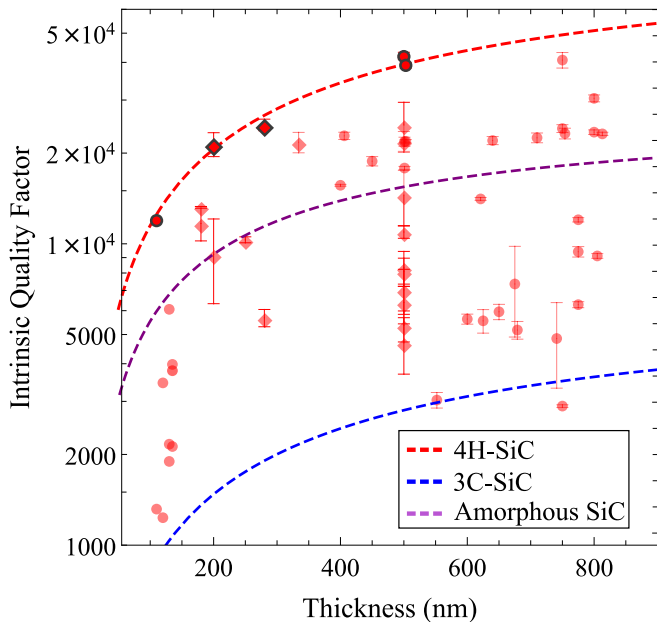


Figure 5. Cumulative extracted intrinsic quality factors for all devices, each string is represented by a red circular point and each cantilever is represented by a red diamond. We fit the upper bounds of our extracted intrinsic quality factors (5 red points with black borders) as a function of thickness using Equation 1, and the fitting parameter α in Equation 3, and plot it using a dashed red line. We add Q_{int} models for amorphous (dashed purple) and crystalline 3C-SiC (dashed blue) for comparison [20, 45].

drawn to other materials in this section are only considering measurements made at room temperature with no surface treatment unless stated otherwise.

To compare our results to current state-of-the-art in silicon carbide, we plot the fitted 4H-SiC intrinsic quality factor model alongside other silicon carbide based nanomechanical loss models in Figure 5 [20, 45]. Compared to 3C-SiC, the 4H polytype upperbound fit has a 23 times higher volumetric quality factor, and 11 times higher surface quality factor. Interestingly, the extracted 4H-SiC surface loss model agrees to within 5% of the surface loss determined in 3C-SiC with crystalline defects removed [20]. It is also apparent that 4H-SiC outperforms amorphous SiC, with 40% less surface damping and five times less volumetric damping. While these are comparisons to the upper bounds of intrinsic quality factors of each material, we additionally note that we measure many resonators with intrinsic quality factors above the limits of both crystalline 3C and amorphous silicon carbide.

The Q_{vol} extracted here is five times larger than the highest reported value for silicon nitride resonators, while the Q_{surf} is 15% greater [39]. A direct comparison with crystalline InGaP is not possible, since measurements have not been made on resonators with similar thicknesses. However, it is possible to extrapolate using our 4H-SiC intrinsic dissipation model. Extrapolating to a

73 nm thick string resonator, as studied in Reference [47], we find that the quality factors should be comparable, with SiC offering a marginal 7% improvement. However we note that the InGaP resonators were measured within a day of fabrication, with degradation of intrinsic quality factors by a factor of four observed over a period of two months. This is likely due to surface effects. Unlike InGaP resonators, we report no decrease in intrinsic quality factor overtime, with stable quality factors over half-year time frames. This suggests that the surface loss of our resonators has reached a steady state.

The intrinsic quality factor of 4H-SiC compares favorably to single-crystal silicon, being about 35% greater [9, 44]. It is about three times larger than the intrinsic quality factor reported for polycrystalline diamond, but an order of magnitude less than single-crystal diamond [9]. Single-crystal diamond nanomechanical resonators with surface treatments achieve even higher intrinsic quality factors [9, 46]. In these studies, a three to five times permanent reduction in surface loss was consistently demonstrated, and as much as an order-of-magnitude reduction in surface loss of some devices was achieved using oxygen-terminated annealing as a surface treatment process. Nonetheless, SiC allows for less challenging and costly fabrication [31, 48]. Additionally, considering the similar crystalline structure of diamond and 4H-SiC, it is conceivable that similar surface treatment techniques may reduce the surface loss in 4H-SiC nanomechanical resonators to a similar magnitude.

Under proper resonator design to effectively remove any radiation loss, and the use of surface treatments, we expect the dissipation of 4H-SiC resonators can be further reduced. For instance, if volumetric damping was the dominant source of dissipation for a 100 nm thick and 3 mm length nanostring composed of 4H-SiC, like those studied here, the dissipation rate would reach as low as 0.2 mHz. This would yield quality factors of 10^8 at room temperature in devices with 310 MPa of tensile stress. Increasing the tensile stress in 4H-SiC resonators to the material yield strength, and using soft-clamped resonator geometries [10, 35, 45], should allow for quality factors of tens of billions at room temperature. This would be comparable to the best cryogenic results using strained silicon nanomechanical resonators at 7 Kelvin [10], as well as the breathing mode of silicon nanomechanical resonators at millikelvin temperatures [49].

V. OBSERVATION AND QUANTIFICATION OF NONLINEAR DISSIPATION

For many applications, understanding solely the linear dissipation of high quality factor nanomechanical resonators is sufficient. However, for other applications such as resonant mass sensing [27] and nanomechanical computing [30], nonlinear dissipation becomes relevant as working drive amplitudes approach the critical amplitude of the resonator, in which nonlinear effects occur. Op-

erating a nanomechanical resonator in the high displacement amplitude regime leads to additional mechanical dissipation as the elastic energy loss attributed to the elongation of the resonator becomes relevant [7, 50]. The nonlinear dissipation rate has been characterized in high stress amorphous silicon nitride [50], but has yet to be determined in crystalline silicon carbide resonators. To investigate this we strongly drive our large aspect ratio string resonators to induce mechanical dissipation nonlinearities. We are able to observe nonlinear dissipation in ringdown measurements as shown in Figure 6.

From this experimental trace, it is evident that a pure linear dissipation model does not sufficiently account for the resonator's faster dissipation at high oscillation amplitudes. To account for the nonlinear dissipation we include a nonlinear damping term introduced in Reference [50] for dissipation-diluted nanomechanical resonators. This allows us to extract the intrinsic linear dissipation rate as well as the nonlinear damping loss parameter. In this example we find the linear mechanical dissipation rate to be 2.7 mHz, linearly damped mechanical $Q = 2.0 \cdot 10^7$ and the nonlinear damping parameter to be $1.1 \cdot 10^{13} \text{ s}^{-1}\text{m}^{-2}$. The nonlinear damping parameter extracted here is somewhat lower than the lowest nonlinear damping parameter that has been experimentally determined for strongly driven, high stress (MHz), soft-clamped silicon nitride resonators of similar thickness ($\approx 1.5 \cdot 10^{13} - 1 \cdot 10^{16} \text{ s}^{-1}\text{m}^{-2}$) [50]. This suggests that 4H-SiC resonators may on average be more linear than similar resonators composed of silicon nitride. As a result, one may drive to higher amplitudes, relative to resonator thickness, and not encounter additional dissipation. This compliments the conclusions regarding the linear dissipation of 4H-SiC, suggesting the material exhibits less linear and nonlinear mechanical dissipation than other materials such as silicon nitride.

VI. CONCLUSIONS

In conclusion we fabricate and characterize nanomechanical cantilever and string resonator devices based on crystalline 4H-SiC. We determine the intrinsic mechanical dissipation to be more than an order-of-magnitude less than previously demonstrated crystalline silicon carbide nanomechanical resonators [19, 20], as well as nearly two orders-of-magnitude lower than bulk crystalline resonators comprised of 4H-SiCOI [25]. This allows us to achieve quality factors as high as $2.0 \cdot 10^7$ at room temperature, and dissipation rates as low as 2.7 mHz in simple string structures. This cumulative result of overall low nanomechanical dissipation in both linear and nonlinear regimes suggests 4H-SiC is particularly useful in applications which operate near the critical amplitude of nanomechanical oscillators. We achieve volumetric damping in crystalline 4H-SiC nanomechanical resonators as low as the predicted fundamental material limit [26]. Despite this, surface loss remains relevant for

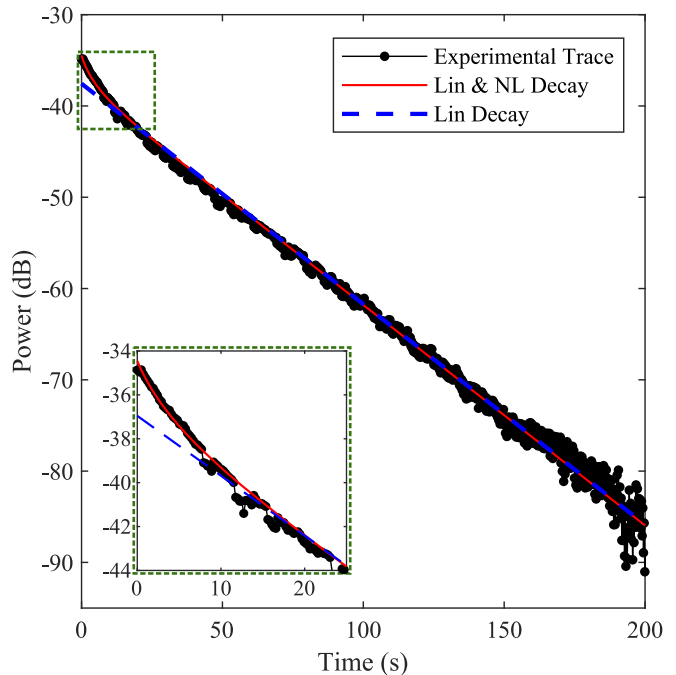


Figure 6. Ringdown measurement and analytical fits of a strongly driven, high-Q nanomechanical string. The black trace represents experimental data for the fundamental transverse mode of a high aspect ratio nanostring. The red trace represents the fit using a linear and nonlinear decay term [50]. The blue dashed trace represents the decay of a damped harmonic oscillator, used to fit the ringdowns of linear nanomechanical resonators.

our devices, offering the possibility to improve performance with appropriate surface treatment. The introduction of high tensile stress close to the material yield strength within 4H-SiC device geometries with higher dissipation dilution and phononic shielding should allow quality factors of tens of billions at room temperature [7].

VII. ACKNOWLEDGMENTS

This work was supported by the Australian Research Council Centres of Excellence for Engineered Quantum Systems (EQUS, CE170100009) and Quantum Biotechnology (CE230100021). This research is partially supported by the Commonwealth of Australia as represented by the Defence Science and Technology Group of the Department of Defence. The work at Stanford was supported by the Vannevar Bush Faculty Fellowship from the Department of Defense.

-
- [1] M. Chien, M. Brameshuber, B. K. Rossboth, G. J. Schütz, and S. Schmid, *Proc Natl Acad Sci USA* **115**, 11150 (2018).
- [2] I. E. Rosłoń, A. Japaridze, P. G. Steeneken, C. Dekker, and F. Alijani, *Nature Nanotechnology* (2022), 10.1038/s41565-022-01111-6.
- [3] F. Massel, T. T. Heikkilä, J.-M. Pirkkalainen, S. U. Cho, H. Saloniemi, P. J. Hakonen, and M. A. Sillanpää, *Nature* **480**, 351 (2011), number: 7377 Publisher: Nature Publishing Group.
- [4] C. T.-c. Nguyen, *IEEE Transactions on Ultrasonics, Ferroelectrics, and Frequency Control* **54**, 251 (2007), conference Name: IEEE Transactions on Ultrasonics, Ferroelectrics, and Frequency Control.
- [5] A. G. Krause, M. Winger, T. D. Blasius, Q. Lin, and O. Painter, *Nature Photonics* **6**, 768 (2012).
- [6] X. Fan, F. Forsberg, A. D. Smith, S. Schröder, S. Wagner, H. Rödjegård, A. C. Fischer, M. Östling, M. C. Lemme, and F. Niklaus, *Nature Electronics* **2**, 394 (2019).
- [7] L. Sementilli, E. Romero, and W. P. Bowen, *Advanced Functional Materials* **32**, 2105247 (2022).
- [8] S. Schmid, L. G. Villanueva, and M. L. Roukes, *Fundamentals of Nanomechanical Resonators* (Springer International Publishing, Cham, 2023).
- [9] Y. Tao, J. M. Boss, B. A. Moores, and C. L. Degen, *Nature Communications* **5**, 3638 (2014), number: 1 Publisher: Nature Publishing Group.
- [10] A. Beccari, D. A. Visani, S. A. Fedorov, M. J. Beryhi, V. Boureau, N. J. Engelsens, and T. J. Kippenberg, *Nature Physics* , 1 (2022), publisher: Nature Publishing Group.
- [11] K. E. Petersen, *Proceedings of the IEEE* **70**, 420 (1982).
- [12] A. L. Ruoff, *Journal of Applied Physics* **50**, 3354 (1979).
- [13] D. M. Lukin, M. A. Guidry, J. Yang, M. Ghezellou, S. Deb Mishra, H. Abe, T. Ohshima, J. Ul-Hassan, and J. Vučković, *Physical Review X* **13**, 011005 (2023).
- [14] E. Janitz, M. K. Bhaskar, and L. Childress, *Optica* **7**, 1232 (2020), publisher: Optical Society of America.
- [15] M. A. Guidry, D. M. Lukin, K. Y. Yang, R. Trivedi, and J. Vučković, *Nature Photonics* **16**, 52 (2022), publisher: Nature Publishing Group.
- [16] D. M. Lukin, C. Dory, M. A. Guidry, K. Y. Yang, S. D. Mishra, R. Trivedi, M. Radulaski, S. Sun, D. Vercurysse, G. H. Ahn, and J. Vučković, *Nature Photonics* **14**, 330 (2020), publisher: Nature Publishing Group.
- [17] S. Castelletto and A. Boretti, *Journal of Physics: Photonics* **2**, 022001 (2020), publisher: IOP Publishing.
- [18] R. Perret, *Power Electronics Semiconductor Devices*, 1st ed. (John Wiley & Sons, Ltd, 2009).
- [19] A. R. Kermany, G. Brawley, N. Mishra, E. Sheridan, W. P. Bowen, and F. Iacopi, *Appl. Phys. Lett.* , 6 (2014).
- [20] E. Romero, V. M. Valenzuela, A. R. Kermany, L. Sementilli, F. Iacopi, and W. P. Bowen, *Physical Review Applied* **13**, 044007 (2020).
- [21] Y. Klas, Thesis, High Q nanomechanical resonators fabricated from crystalline silicon carbide (2022).
- [22] X. Huang, C. Zorman, M. Mehregany, and M. Roukes, in *TRANSDUCERS '03. 12th International Conference on Solid-State Sensors, Actuators and Microsystems. Digest of Technical Papers (Cat. No.03TH8664)*, Vol. 1 (IEEE, Boston, MA, USA, 2003) pp. 722–725.
- [23] F. La Via, A. Severino, R. Anzalone, C. Bongiorno, G. Litrico, M. Mauceri, M. Schoeler, P. Schuh, and P. Wellmann, *Mater Sci Semicond Process Wide band gap semiconductors technology for next generation of energy efficient power electronics*, **78**, 57 (2018).
- [24] R. Anzalone, G. Litrico, N. Piluso, R. Reitano, A. Alberti, P. Fiorenza, S. Coffa, and F. La Via, *J. Cryst. Growth* **473**, 11 (2017).
- [25] B. Hamelin, J. Yang, A. Daruwalla, H. Wen, and F. Ayazi, *Scientific Reports* **9**, 18698 (2019).
- [26] M. F. Ashby, *Acta Metallurgica* **37**, 1273 (1989).
- [27] K. L. Ekinci, Y. T. Yang, and M. L. Roukes, *Journal of Applied Physics* **95**, 2682 (2004).
- [28] Y. T. Yang, C. Callegari, X. L. Feng, K. L. Ekinci, and M. L. Roukes, *Nano Lett.* **6**, 583 (2006).
- [29] N. P. Mauranyapin, E. Romero, R. Kalra, G. Harris, C. G. Baker, and W. P. Bowen, *Physical Review Applied* **15**, 054036 (2021), publisher: American Physical Society.
- [30] E. Romero, N. P. Mauranyapin, T. M. F. Hirsch, R. Kalra, C. G. Baker, G. I. Harris, and W. P. Bowen, “Scalable nanomechanical logic gate,” (2022), arXiv:2206.11661 [cond-mat, physics:physics].
- [31] D. M. Lukin, M. A. Guidry, and J. Vučković, *Optics and Photonics News* **32**, 34 (2021).
- [32] S. J. Whiteley, G. Wolfowicz, C. P. Anderson, A. Bourassa, H. Ma, M. Ye, G. Koolstra, K. J. Satzinger, M. V. Holt, F. J. Heremans, A. N. Cleland, D. I. Schuster, G. Galli, and D. D. Awschalom, *Nature Physics* **15**, 490 (2019).
- [33] E. Cook, M. Tomaino-Iannucci, J. Bernstein, M. Weinberg, J. Choy, K. Hobart, L. Luna, M. Tadjer, R. Myers-Ward, F. Kub, Y. Yang, and I. Flader, in *2018 Solid-State, Actuators, and Microsystems Workshop Technical Digest* (Transducer Research Foundation, Hilton Head, South Carolina, USA, 2018) pp. 364–365.
- [34] M. J. Beryhi, A. Beccari, R. Groth, S. A. Fedorov, A. Arabmoheghi, T. J. Kippenberg, and N. J. Engelsens, *Nature Communications* **13**, 3097 (2022), number: 1 Publisher: Nature Publishing Group.
- [35] A. H. Ghadimi, S. A. Fedorov, N. J. Engelsens, M. J. Beryhi, R. Schilling, D. J. Wilson, and T. J. Kippenberg, , 6 (2018).
- [36] B. J. M. Hausmann, B. Shields, Q. Quan, P. Maletinsky, M. McCutcheon, J. T. Choy, T. M. Babinec, A. Kubanek, A. Jacoby, M. D. Lukin, and M. Lončar, *Nano Letters* **12**, 1578 (2012), publisher: American Chemical Society.
- [37] J. Yang, K. Van Gasse, D. M. Lukin, M. A. Guidry, G. H. Ahn, A. D. White, and J. Vučković, “Titanium:Sapphire-on-insulator for broadband tunable lasers and high-power amplifiers on chip,” (2023), arXiv:2312.00256 [physics, physics:quant-ph].
- [38] S. Schmid, K. D. Jensen, K. H. Nielsen, and A. Boisen, *Physical Review B* **84**, 165307 (2011).
- [39] L. Villanueva and S. Schmid, *Physical Review Letters* **113**, 227201 (2014).
- [40] A. R. Kermany, J. S. Bennett, G. A. Brawley, W. P. Bowen, and F. Iacopi, *J. Appl. Phys* **119**, 055304 (2016).
- [41] S. A. Fedorov, N. J. Engelsens, A. H. Ghadimi, M. J. Beryhi, R. Schilling, D. J. Wilson, and T. J. Kippenberg, *Physical Review B* **99**, 054107 (2019).

- [42] P. Sadeghi, M. Tanzer, S. L. Christensen, and S. Schmid, *Journal of Applied Physics* **126**, 165108 (2019).
- [43] Jinling Yang, T. Ono, and M. Esashi, *Journal of Microelectromechanical Systems* **11**, 775 (2002).
- [44] K. Y. Yasumura, T. D. Stowe, E. M. Chow, T. Pfafman, T. W. Kenny, B. C. Stipe, and D. Rugar, *J. Microelectromech. S.* **9**, 117 (2000).
- [45] M. Xu, D. Shin, P. M. Sberna, R. van der Kolk, A. Cupertino, M. A. Bessa, and R. A. Norte, *Advanced Materials* **n/a**, 2306513 (2023).
- [46] Y. Tao, P. Navaretti, R. Hauert, U. Grob, M. Poggio, and C L Degen, *Nanotechnology* **26**, 465501 (2015).
- [47] S. K. Manjeshwar, A. Ciers, F. Hellman, J. Bläsing, A. Strittmatter, and W. Wiczorek, *Nano Letters* **23**, 5076 (2023), publisher: American Chemical Society.
- [48] L. V. H. Rodgers, L. B. Hughes, M. Xie, P. C. Maurer, S. Kolkowitz, A. C. Bleszynski Jayich, and N. P. De Leon, *MRS Bulletin* **46**, 623 (2021).
- [49] G. S. MacCabe, H. Ren, J. Luo, J. D. Cohen, H. Zhou, A. Sipahigil, M. Mirhosseini, and O. Painter, *Science* **370**, 840 (2020), publisher: American Association for the Advancement of Science.
- [50] L. Catalini, M. Rossi, E. C. Langman, and A. Schliesser, *Physical Review Letters* **126**, 174101 (2021).
- [51] M. Bückle, *Nanomechanical Systems Based on Tensile-Stressed Crystalline Indium Gallium Phosphide*, Ph.D. thesis (2020).
- [52] X. Yao, D. Hoch, and M. Poot, *Physical Review B* **106**, 174109 (2022).
- [53] M. Bückle, Y. S. Klaß, F. B. Nägele, R. Braive, and E. M. Weig, *Physical Review Applied* **15**, 034063 (2021).
- [54] S. S. Verbridge, D. F. Shapiro, H. G. Craighead, and J. M. Parpia, *Nano Letters* **7**, 1728 (2007).

Table I. Comparison of Silicon Carbide nano/bulk mechanical resonators.

Ref	Frequency	Q ($\times 10^6$)	$\Gamma/2\pi$ (mHz)	Type
[25]	5.3 MHz	18	290	4H-SiCOI Bulk
[45]	895 kHz	198	4.5	Amorphous Nano
[20]	211 kHz	1.74	121	3C-SiC Nano
[19]	280 kHz	2.9	90	3C-SiC Nano
This Work	53 kHz	20	2.7	4H-SiCOI Nano

VIII. SUPPLEMENTARY

A. Comparing to other SiC devices

Table I summarizes best reported experimental parameters for a variety of silicon carbide resonators. This includes both amorphous/crystalline as well as nanomechanical/bulk acoustic wave resonators.

B. Overhang Effect Towards Dissipation Dilution Factor of String Resonators

As can be seen in Figure 1(a-b), our devices possess overhang near the clamping points due to undercut during the fabrication process. Therefore they are not entirely perfectly clamped beams and to conduct a thorough analysis of intrinsic quality factors we summarize the effect of overhang towards the dissipation dilution factor here. We omit the analysis for cantilevers due to the lack of tensile stress (one clamping point). We infer the undercut to be 25 microns based on SEM images, and is fixed for each string regardless of the strings dimensions.

First we model the stationary solution of our uniform strings of many different lengths since the proportion of undercut to total string length is different across our entire sample set. This can be seen in Figure 7, where the deposition (unrelaxed) stress is 220 MPa. In many approximations the relaxed tensile stress is not determined by the thickness [35, 41]. This was confirmed via FEM for the sake of checking accuracy of the model and this assumption. As expected we find the fixed overhang makes a larger difference in the relaxed stress of shorter strings, specifically a 14% difference for strings with overhang compared to perfectly clamped strings. The relaxed stress becomes very similar to the model of a perfectly clamped uniform string at longer lengths (within 4% at 1mm length). Overall, we find the presence of overhang increases the tensile stress of the devices which supports others work [51–53].

We then calculate the eigenfrequency of the fundamental transverse mode for the entire range of lengths. Since the frequency of a stressed string scales as the square root of stress (Equation 2) the overhang should make a smaller impact in resonance frequency. Indeed, we find that the resonance frequencies of strings with overhang to be very similar to those without overhang. Previous

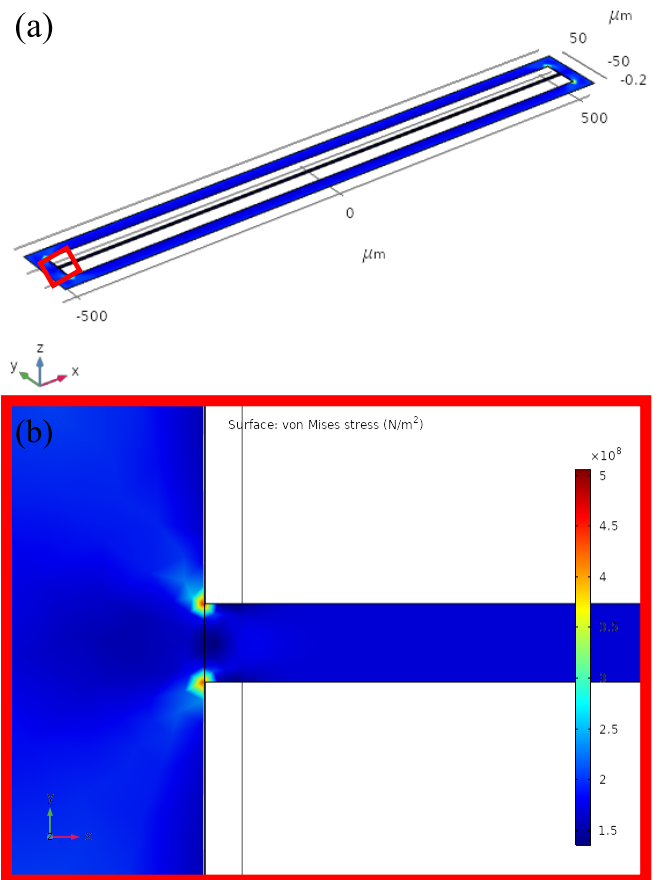


Figure 7. (a) Simulated geometry of uniform string resonators with a rectangular frame, as closely representing actual device release from undercut etching. (b) Stationary solution of one clamping point of string resonator under tensile prestress of 220 MPa.

work studying the effect of overhang on the frequency of resonators has also shown similar results [54].

Following this, we then calculate the dissipation dilution factor for our mean string thickness across a variety of lengths that cover our entire data set. We reach a similar conclusion that strings with larger undercut relative to overall length are most affected. As a whole we observed increased dissipation dilution for the simulated overhang geometry in Figure 7(a). We attribute this to the localization of relaxed stress near the strings clamping points as shown in Figure 7(b). We then consider overhang for the entire range of thicknesses and lengths used for these devices and calculate the corrected dissipation dilution value for each device size. We plot these results in Figure 8, directly comparing expected dissipation dilution values for uniform strings with (blue) and without (black) overhang. For comparison, we bound the data within an expected dissipation dilution value range (gray shaded region) using Equation 4. We determine this expected range for our resonators using the data set's mean stress, as well as the shortest and longest resonator length as a function of thickness. We observe that ac-

counting for overhang allows us to encompass every data point within the expected range of dilution values. For the approximations of intrinsic Q in Figure 5, we use the dissipation dilution terms accounting for overhang.

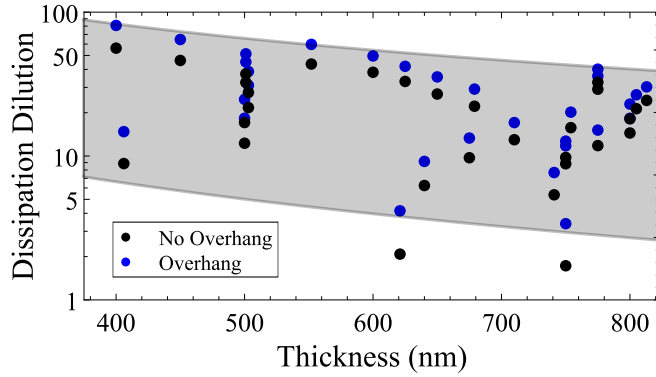


Figure 8. Change in dissipation dilution factor for strings which have no overhang (black) and strings with overhang (blue). The gray bounded region represents the range where we'd expect the dissipation dilution values to be given the data set's mean stress, and lengths of the shortest and longest resonators in the data set.